

# Cabibbo suppressed hyperon production off nuclei induced by antineutrinos

M. Benitez Galan,<sup>1,\*</sup> L. Alvarez-Ruso,<sup>2</sup> M. Rafi Alam,<sup>3</sup> I. Ruiz Simo,<sup>4,†</sup> and M.J. Vicente Vacas<sup>5</sup>

<sup>1</sup>*Departamento de Física Atómica, Molecular y Nuclear,  
Facultad de Ciencias, Universidad de Granada, E-18071, Granada, Spain*

<sup>2</sup>*Instituto de Física Corpuscular (IFIC), Consejo Superior de  
Investigaciones Científicas (CSIC), E-46980 Paterna, Valencia, Spain*

<sup>3</sup>*Department of Physics, Aligarh Muslim University, Aligarh-202 002, India*

<sup>4</sup>*Departamento de Física Atómica, Molecular y Nuclear and Instituto  
Interuniversitario Carlos I de Física Teórica y Computacional,  
Facultad de Ciencias, Universidad de Granada, E-18071, Granada, Spain*

<sup>5</sup>*Departamento de Física Teórica and Instituto de Física Corpuscular (IFIC),  
Centro Mixto UVEG-CSIC, Valencia E-46071, Spain*

In this work we study the production of  $\Sigma$  and  $\Lambda$  hyperons in strangeness changing  $\Delta S = -1$  charged current interactions of muon antineutrinos on nuclear targets. At the nucleon level, besides quasielastic scattering we consider the inelastic mechanism in which a pion is produced alongside the hyperon. Its relevance for antineutrinos with energies below 2 GeV is conveyed in integrated and differential cross sections. We observe that the distributions on the angle between the hyperon and the final lepton are clearly different for quasielastic and inelastic processes. Hyperon final state interactions, modeled with an intranuclear cascade, lead to a significant transfer from primary produced  $\Sigma$ 's into final  $\Lambda$ 's. They also cause considerable energy loss, which is apparent in hyperon energy distributions. We have investigated  $\Lambda$  production off  $^{40}\text{Ar}$  in the conditions of the recently reported MicroBooNE measurement. We find that the  $\Lambda\pi$  contribution, dominated by  $\Sigma^*(1385)$  excitation, accounts for about one third of the cross section.

## I. INTRODUCTION

The flavour changing charged currents of the Standard Model connect up and strange quarks,  $W^- u \rightarrow s$ . Weak interactions on nucleons can then lead to strange hadrons and, in particular, hyperons in the final state:  $W^- N \rightarrow Y$ . The amplitudes for such  $\Delta S = -1$  processes are proportional to the sine of the Cabibbo angle [1] or  $V_{us} = 0.22500 \pm 0.00067$  [2] and are therefore suppressed with respect to their counterparts involving only  $u \leftrightarrow d$  transitions with  $V_{ud} = 0.97435 \pm 0.00016$  [2]. Nevertheless, the form factors that characterize the electroweak  $N \rightarrow Y$  current encode relevant details about the hadronic structure, SU(3) breaking corrections, G-parity or time-reversal invariance violation. They are also a valuable input for the determination of CKM matrix elements.

On the theoretical side there has been a continuing effort trying to obtain the relevant axial and vector form factors [3–5] and the possible SU(3) breaking effects from QCD and QCD-inspired models. For instance, lattice QCD [6–8], chiral perturbation theory [6, 9–12],  $1/N_c$  expansions [13–15] or quark models [16–19] have been used. Nonetheless, our knowledge of these form factors is still not satisfactory, in part due to the scarcity of experimental information, which comes mostly from hyperon semileptonic decays and is thus restricted to very small momentum transfers.

On the other hand, the reaction  $\bar{\nu} + N \rightarrow l^+ + Y$ ,

which better probes the momentum transfer dependence of the  $N \rightarrow Y$  form factors has been insufficiently explored. Indeed, at the moment, there is just a handful of  $\Lambda$  and  $\Sigma$  production events observed at several bubble chambers: Gargamelle, filled with freon [20, 21] and propane [22], ANL with deuterium [23], BNL with hydrogen [24, 25], Fermilab with a heavy neon-hydrogen mixture [26] or with deuterium [27] and SKAT, filled with freon [28]. In spite of the low statistics and incoming flux uncertainties, these experiments could estimate low-energy ( $E_\nu < 20$  GeV) cross sections for  $\Delta S = -1$  single  $\Lambda$ ,  $\Sigma$ ,  $\Delta S = 0$   $\Lambda K$  production and  $YX$ ,  $YKX$ , where  $X$  stands for additional hadrons. At higher energies, some cross sections and rates, but also hyperon yields and polarization measurements have been performed with bubble chambers (see Ref. [29] for a comprehensive list of references) and by the NOMAD experiment [30, 31].

Recently, the first measurement of  $\bar{\nu}_\mu + ^{40}\text{Ar} \rightarrow \mu^+ + \Lambda + X$ , where  $X$  denotes the final state content without strangeness, has been reported by the MicroBooNE Collaboration [32]. So far only five  $\Lambda$  events have been identified analyzing the exposure of the MicroBooNE liquid argon detector to the off-axis NUMI beam at FNAL. Fortunately, the situation is bound to improve with the large data sample collected by MicroBooNE and still awaiting analysis [32] and the much larger one expected at the SBND detector [33, 34].

The fact that the constituents of the baryonic matter present in (anti)neutrino detectors are light  $u$  and  $d$  quarks, while the corresponding antiquarks are only present in the sea of  $q\bar{q}$  pairs, implies that  $\Delta S = -1$   $W^- u \rightarrow s$  processes induced by  $\bar{\nu}$  are very different from the  $\Delta S = 1$ ,  $W^+ \bar{u} \rightarrow \bar{s}$  ones induced by  $\nu$ . In

\* mbenitezgalan@ugr.es

† ruizsig@ugr.es

particular, only antineutrino interactions can trigger the production of single-hyperons and strange baryon resonances. The consequence of this  $\nu/\bar{\nu}$  asymmetry for CP-violation searches has not been investigated although it has been pointed out that, owing to their weak decays,  $Y \rightarrow \pi N$ , hyperons become an additional source of pions in  $\bar{\nu}$  interactions [35–37]. Furthermore, if sufficiently determined by experiments, hyperon production could be used to constrain the  $\bar{\nu}$  contamination in a  $\nu$  beam [32].

As apparent from the experimental outline above,  $\bar{\nu}$  scattering on single nucleons leads to a variety of final states. First, starting from low energies, there are  $\Delta S = -1$  quasielastic (QE) interactions,  $\bar{\nu} + N \rightarrow l^+ + Y$ . The formalism to write the QE cross section in terms of transition form factors, relating the later to the nucleon ones by flavor SU(3) rotations, was laid down in Ref. [3] and followed closely in subsequent studies [35, 38, 39]. Second, with a slightly higher energy threshold, an additional pion could be produced,  $\bar{\nu} + N \rightarrow l^+ + Y + \pi + X$ . For this process, which we label as  $Y\pi$ , a model in terms of light pseudoscalar mesons and baryon octets as effective degrees of freedom was proposed in Ref. [40]. It has been improved and extended to include the lowest-lying decuplet resonances in Ref. [41]. This study finds that the  $\Sigma(1385) 3/2^+$  intermediate state plays a prominent role in  $\Lambda\pi$  production. A specific reaction mechanism in which the  $\Lambda(1405) 1/2^-$  is excited, contributing to the  $\Sigma\pi$  final state has also been considered [42]. In addition, two and more pions can accompany the hyperon as the energy further increases. Another possible  $\Delta S = -1$  process is  $\bar{\nu} + N \rightarrow l^+ + N' + \bar{K}$  [40, 43]; it can lead to hyperon production in nuclei (introduced below) through  $\bar{K} N \rightarrow Y\pi$  final state interactions. Next we have,  $\Delta S = 0$ ,  $\bar{\nu} + N \rightarrow l^+ + Y + K$ . It has been theoretically studied in Born approximations [44, 45] and, more recently, accounting for unitarization in coupled channels [46]. Let us recall that the production of hyperons by  $\Delta S = -1$  channels (QE,  $Y\pi$ ) is suppressed as compared to the  $\Delta S = 0$  ones by a factor  $(V_{us}/V_{ud})^2 \approx 0.05$ . However, this reduction is more than compensated at low energies,  $E_{\bar{\nu}} < 2$  GeV, by the fact that the associated production of hyperons requires the creation of an additional kaon and is, therefore, strongly reduced by phase space.

Neutrino experiments rely on heavy targets to increase the available statistics. Indeed, most hyperons produced in the laboratory arise from scattering on nuclear targets, which introduces significant complications for the analysis and interpretation of experimental results. In this instance, the weak interaction takes place on a bound nucleon from a nuclear target while the scattering process leaves the residual nucleus in an excited state. The initial nucleon has been described with the global [47] and local [35, 47, 48] Fermi gas approximations and taking the nuclear mean field and nucleon-nucleon correlations into account [48]. Additionally, it must be considered that hyperons produced in the primary scattering propagate through the nucleus undergoing final state inter-

actions (FSI), where they can collide with the nucleons, change direction, lose energy or even turn into a different hyperon species before getting out of the nucleus and being detected. Hyperons can also be created by  $\bar{K}N$  FSI, as mentioned above, or by high-energy pions via  $\pi N \rightarrow Y K$  secondary scattering. These FSI, which can be handled with semiclassical methods [35, 47–49], have strong impact on the observables, sizably exceeding the influence of the nuclear initial state treatment [48].

Unlike QE hyperon production,  $Y\pi$  mechanisms have not yet been studied in nuclei. In this context, it is worth noticing that there is no QE  $\Sigma^+$  production on a single nucleon. This hyperon could only appear due to nuclear FSI. However, allowing for the presence of additional pions, namely the  $Y\pi$  channel, the  $\Sigma^+$  hyperon can be directly produced on a single proton.

In the present study of the  $\Lambda$  and  $\Sigma$  production off nuclei induced by charged current interactions of muon antineutrinos, the inelastic  $Y\pi$  channel is considered alongside the QE one. By restricting ourselves to the  $E_{\bar{\nu}} \lesssim 2$  GeV range of Laboratory energies, which is probed at MicroBooNE and SBND, we can neglect hyperon production accompanied by more than one pion, the associated  $YK$  reaction channel and secondary hyperon production induced by  $\bar{K}$ . We include FSI accounting for the propagation of hyperons in the nuclear medium with the help of a Monte Carlo simulation. The model is applied to the recent MicroBooNE measurement [32]. We find that under the phase space restrictions imposed by detection thresholds, the  $Y\pi$  mechanism becomes particularly important.

The structure of this article is as follows: in Sec. II we present the formalism employed to describe QE and  $Y\pi$  primary reactions on nucleons and nuclei; hyperon FSI are discussed in Sec. II E. Various observables: cross sections, energy and angular distributions are described in Sec. III, together with our analysis of the MicroBooNE measurement. Finally, in Sect. IV we summarize the main conclusions of this study.

## II. FORMALISM

In this section, we describe the formalism employed to obtain the total and differential cross sections for QE and inelastic ( $Y\pi$ ) hyperon production on nucleons and nuclei<sup>1</sup>. As nuclear effects, our approach includes Fermi motion of the target nucleons and FSI of the emitted hyperons. Fermi motion is accounted for using the Fermi gas model with the local density approximation. FSI is implemented within the model of intranuclear re-interaction

<sup>1</sup> Most of the formalism is readily available elsewhere [35, 41], where more details can be found. Here, for the sake of clarity, we provide a brief outline unifying the notation of previous works.

of the primary produced hyperons with the nucleons of the nuclei described in Ref. [35]<sup>2</sup>.

### A. Quasielastic hyperon production on nucleons

This reaction is the main source of strange baryons at low energies with antineutrino beams. As a consequence of the  $\Delta S = \Delta Q$  selection rule, the allowed channels are

$$\bar{\nu}_l(k) + p(p) \rightarrow l^+(k') + \Lambda(p_Y), \quad (1)$$

$$\bar{\nu}_l(k) + p(p) \rightarrow l^+(k') + \Sigma^0(p_Y), \quad (2)$$

$$\bar{\nu}_l(k) + n(p) \rightarrow l^+(k') + \Sigma^-(p_Y), \quad (3)$$

where  $k, p, k', p_Y$  denote the antineutrino, nucleon, lepton and hyperon four-momenta, respectively.

The cross section on a free nucleon can be written as

$$d\sigma_N^{\text{QE}} = \frac{1}{(2\pi)^2} \frac{1}{2(s - m_N^2)} \delta^4(k + p - k' - p_Y) \frac{d^3k'}{2E_l(\mathbf{k}')} \frac{d^3p_Y}{2E_Y(\mathbf{p}_Y)} \overline{\sum} |\mathcal{M}|^2, \quad (4)$$

where  $s = (k + p)^2$  and  $m_N$  stands for the nucleon mass. The outgoing particle energies obey the on-shell conditions  $E_Y = \sqrt{m_Y^2 + \mathbf{p}_Y^2}$  and  $E_l = \sqrt{m_l^2 + \mathbf{k}'^2}$ , in terms of the corresponding masses  $m_{Y,l}$  and three-momenta  $\mathbf{p}_Y, \mathbf{k}'$ . The overlined summation symbol denotes the sum over the final fermion polarizations and the average over the initial ones. The scattering amplitude matrix element is given by

$$\mathcal{M} = \frac{G_F}{\sqrt{2}} \bar{v}(k) \gamma_\mu (1 - \gamma^5) v(k') J_H^\mu \quad (5)$$

where  $\bar{v}$  and  $v$  are the lepton spinors;  $G_F = 1.1664 \times 10^{-5} \text{ GeV}^{-2}$  [2] is the Fermi constant. The hadronic current

$$J_H^\mu = V_{us} \langle Y | \bar{s} \gamma^\mu (1 - \gamma^5) u | N \rangle, \quad (6)$$

can be expressed in terms of three vector and three axial-vector transition form factors. Assuming SU(3) flavor symmetry, they can be related to their nucleon counterparts. We follow the specific choices of Ref. [35] where the reader is referred for details.

### B. Hyperon-pion production on nucleons

The process under consideration now is generically given by

$$\bar{\nu}_l(k) + N(p) \rightarrow l^+(k') + \pi(p_m) + Y(p_Y), \quad (7)$$

where, in addition to the previously defined ones,  $p_m$  denotes the pion four-momentum. For  $N = p$  the allowed  $Y\pi$  final states are  $\Lambda\pi^0, \Sigma^0\pi^0, \Sigma^-\pi^+$  and  $\Sigma^+\pi^-$  while for  $N = n$ ,  $Y\pi = \Lambda\pi^-, \Sigma^0\pi^-$  and  $\Sigma^-\pi^0$ .

The differential cross section for this reaction on free nucleons is

$$d\sigma_N^{Y\pi} = \frac{1}{(2\pi)^5} \frac{1}{2(s - m_N^2)} \delta^4(k + p - k' - p_Y - p_m) \frac{d^3k'}{2E_l(\mathbf{k}')} \frac{d^3p_m}{2E_m(\mathbf{p}_m)} \frac{d^3p_Y}{2E_Y(\mathbf{p}_Y)} \overline{\sum} |\mathcal{M}|^2, \quad (8)$$

where the matrix element is also given by Eq. 5 but with a hadronic inelastic current

$$J_H^\mu = V_{us} \langle Y\pi | \bar{s} \gamma^\mu (1 - \gamma^5) u | N \rangle, \quad (9)$$

which encompasses Born terms derived using the lowest order effective Lagrangian including the low-lying baryon octet. The  $N-Y$  vertices incorporate the same transition form factors that characterize QE hyperon production. The baryon decuplet enters via a  $u$ -channel contribution of the  $\Delta(1232)$  and the excitation of the  $\Sigma^*(1385)$  which decays to  $\Sigma\pi$  and, predominantly, to  $\Lambda\pi$ . The octet-to-decuplet form factors are expressed in terms of the  $N-\Delta(1232)$  ones using SU(3) symmetry. For full details, the reader is referred to [41].

### C. The nuclear cross section

The cross section on a nucleus of mass number  $A$  and charge  $Z$  is given by the integral over all possible nucleon momenta in the Fermi sea

$$d\sigma_A^i = \int d^3r \, 2 \int \frac{d^3p}{(2\pi)^3} n_N(\mathbf{p}, \mathbf{r}) d\sigma_N^i \quad (10)$$

where  $n_N(\mathbf{p}, \mathbf{r}) = \theta(k_F^N(r) - |\mathbf{p}|)$  is the occupation number of the initial nucleon of type  $N = p, n$  with momentum  $\mathbf{p}$ . Its dependence on the radial coordinate comes from the Fermi momentum

$$k_F^N(r) = [3\pi^2 \rho_N(r)]^{1/3}, \quad (11)$$

defined in terms of the local density of protons or neutrons. For the proton densities we take empirical parametrizations from Ref. [50], re-scaling them by a factor of  $(A - Z)/Z$  for neutrons. Index  $i$  stands for one of the possible QE or  $Y\pi$  reactions. In the QE case only one of the nucleon types contributes for a given hyperon species. In other words,  $N = p, n$  for primary produced  $\Lambda, \Sigma^0, \Sigma^-$  respectively. In the case of the  $Y\pi$  reaction, for a given hyperon both protons and neutrons contribute (with the charge of the outgoing pion changed accordingly) except  $\Sigma^+$  hyperons that are primary produced only on protons.

<sup>2</sup> A very similar approach was adopted in Ref. [48].

### D. Hyperon nuclear potentials

Hyperons are produced in the mean field of the nucleus. Such hyperon nucleus potentials, and hyperon strong interactions in general, are not very well known. There is a consensus in the literature that the  $\Lambda$  nuclear potential is attractive, with a depth of around 30 MeV [51, 52]. The  $\Sigma$  potential is difficult to determine. Even its sign is not established although repulsive values inside the nucleus are currently preferred [53, 54]. We disregard the latter but take into account the effect of a  $\Lambda$  potential, parametrized as

$$V_\Lambda(r) = -30 \text{ MeV} \frac{\rho(r)}{\rho(0)}, \quad (12)$$

with  $\rho = \rho_p + \rho_n$ , on the hyperon propagation through the nucleus and FSI.

### E. Final State Interaction

In a semiclassical language, hyperons, initially produced in QE or  $Y\pi$  processes on target nucleons, propagate through the nucleus changing hyperon species and/or energy and direction via  $Y + N \rightarrow Y' + N'$  interactions. Next, we describe the Monte Carlo simulation accounting for these FSI and the  $\Lambda$  potential.

The propagation of a given hyperon, produced in one of the possible primary interactions of a  $\bar{\nu}$  with laboratory energy  $E_{\bar{\nu}}$ , starts at a random position  $\mathbf{r}_0$  inside the nucleus. The momentum of the initial nucleon is generated isotropically, with  $|\mathbf{p}| < k_F^N(r)$ . Those of the outgoing lepton,  $\mathbf{k}'$ , and pion,  $\mathbf{p}_m$ , (if applicable) are also randomly generated after energy conservation is imposed. The hyperon momentum at this initial coordinate is constrained by momentum conservation as  $\mathbf{p}_Y = \mathbf{k} - \mathbf{k}' + \mathbf{p}$  (QE) or  $\mathbf{p}_Y = \mathbf{k} - \mathbf{k}' + \mathbf{p} - \mathbf{p}_m$  ( $Y\pi$ ). In the case of the  $\Lambda$ , this  $\mathbf{p}_\Lambda$  is regarded as the asymptotic momentum the hyperon would have in the absence of FSI. To account for the potential the  $\Lambda$  initial energy is increased by  $-V_\Lambda(r_0)$  and the absolute value of its momentum is adjusted as

$$|\mathbf{p}_\Lambda|^2(\mathbf{r}_0) = \left[ \sqrt{m_\Lambda^2 + \mathbf{p}_\Lambda^2} - V_\Lambda(r_0) \right]^2 - m_\Lambda^2 \quad (13)$$

In this way, the  $\Lambda$  hyperon is propagated as an on-shell particle [47]. Functions

$$\frac{d\sigma_A^i}{d^3r d^3p d^3k'} \left( \frac{d\sigma_A^i}{d^3r d^3p d^3k' d^3p_m} \right)$$

provide the weights assigned to the QE ( $Y\pi$ ) events of channel  $i$ .

Once the initial properties of the event have been fixed, the simulation proceeds by moving the hyperon along a trajectory determined by the classical Hamilton equations of motion. For  $\Sigma$ , the absence of potential implies

that this trajectory is just a straight line along the hyperon's momentum direction. The travelled distance  $dl$  is chosen such that  $P_Y dl \ll 1$ . Here  $P_Y$  is the probability per unit length of hyperon-nucleon interaction at point  $\mathbf{r}$ , given by

$$P_Y(r) = \sum_{f,f'} \{ \sigma_{Yn \rightarrow f}(\bar{s}) \rho_n(r) + \sigma_{Yp \rightarrow f'}(\bar{s}) \rho_p(r) \}, \quad (14)$$

where the sum is performed over all possible hyperon-nucleon final states. The integrated elastic and quasielastic  $YN$  cross sections  $\sigma_{YN \rightarrow Y'N'}$  were extracted from the available experimental data and conveniently parametrized in Ref. [35]. They are evaluated at a  $YN$  invariant energy  $\bar{s}$  averaged over the local Fermi sea. At this stage, a random number  $x \in [0, 1]$  is generated. If  $x > P_Y dl$  there is no interaction and the hyperon moves further a distance  $dl$ . If not, an interaction has occurred and a new  $Y'N'$  final state is randomly chosen among the allowed ones according to their respective probabilities. Next, the momentum of the new  $Y'$  hyperon is generated: from the  $YN$  invariant mass, calculated for an initial nucleon at rest, the center-of-mass (CM) momenta of the final hyperon and nucleon are obtained; their (back to back) directions are randomly generated assuming an isotropic CM angular distribution. Then, the two momenta are boosted to the Laboratory frame. If the  $N'$  momentum is below the local Fermi level, the event is Pauli blocked: the interaction does not actually take place and the original hyperon is propagated a distance  $dl$  through its trajectory. Otherwise, one has a new hyperon  $Y'$  with a new momentum.

Following Ref. [47] we implement further adjustments in this algorithm, which are required to account for the  $\Lambda$  potential. In case of a  $\Lambda N \rightarrow \Lambda N$  interaction one should check that after the collision  $\sqrt{m_\Lambda^2 + \mathbf{p}_\Lambda^2} + V_\Lambda(r) > m_\Lambda$ . Otherwise, the  $\Lambda$  is trapped in the attractive potential, its propagation is ceased and the hyperon is not counted as an asymptotic final state.<sup>3</sup> Next, if a secondary  $\Lambda$  is born in a  $\Sigma N \rightarrow \Lambda N'$  interaction, its energy is increased by  $-V_\Lambda(r)$  and its momentum re-adjusted according to Eq. 13 (with  $r$  instead of  $r_0$ ), just as for a primarily produced  $\Lambda$  hyperon. Finally, after a  $\Lambda N \rightarrow \Sigma N'$  FSI, the  $\Sigma$  energy has to be decreased by  $V_\Lambda(r)$  and its momentum adjusted to correspond to an on-shell  $\Sigma$  with the analogous of Eq. 13 for a  $\Sigma$  at position  $\mathbf{r}$ , unless  $\sqrt{m_\Sigma^2 + \mathbf{p}_\Sigma^2} + V_\Lambda(r) < m_\Sigma$ . In the latter case, no  $\Sigma$  hyperon can actually be created, so the interaction is disregarded and the original  $\Lambda$  continues its propagation.

<sup>3</sup> A fraction of bound  $\Lambda$  hyperons decays weakly to  $p\pi^-$  and could be experimentally measured from these decay products. However, the distortion of the emitted pion and nucleon in the nucleus will render the  $\Lambda$  identification difficult. Furthermore, detection thresholds will hinder the measurement. In particular, as discussed below, low-energy  $\Lambda$  are undetectable at MicroBooNE. Last but not least, one should recall that a semiclassical cascade is unsuitable to describe the formation and decay of  $\Lambda$  hypernuclei.



Although the main purpose of this study is to evaluate the total hyperon production, it would be of interest to consider as well the FSI of pions produced via the  $Y\pi$  processes. If such pions were detected, it would lead to a better understanding of the underlying physics.

The primary interaction occurs on the whole volume of the nucleus and, thus, pions in their way out could scatter, changing energy, direction, charge, or be absorbed. A comprehensive calculation of these effects would require a cascade simulation for both hyperons and pions. This is beyond of the scope of this work but the effect of pion absorption can be reasonably estimated using an eikonal approximation. This approach has been successfully used in the analysis of several pion production processes in nuclei induced by pions [55] or neutrinos [56, 57]. In this approximation, the probability for a pion to escape from the nucleus is given by

$$P_{\text{no abs}} = \exp \left[ -\frac{1}{|\mathbf{p}_m|} \int_0^\infty \text{Im } \Pi_{\text{abs}} \left( \mathbf{r} + \lambda \frac{\mathbf{p}_m}{|\mathbf{p}_m|} \right) d\lambda \right] \quad (15)$$

where  $\mathbf{r}$  denotes the pion production point;  $\text{Im } \Pi_{\text{abs}}$  is the fraction of the imaginary part of the pion selfenergy in the nuclear medium, which corresponds to pion absorption. For our estimates, we take this selfenergy from Refs. [58, 59].

### III. RESULTS

We present several results for hyperon production off nuclei induced by antineutrino beams. As discussed in the introduction, our predictions for hyperon production are reliable as far as the  $\Delta S = -1$  QE and  $Y\pi$  processes are prevalent. This restricts the incoming neutrino energies to  $E_{\bar{\nu}} \lesssim 2$  GeV. The  $\Delta S = 0$  is also suppressed for measurements where no kaons are allowed in the final state. Once the QE mechanism has been considered in earlier studies, whose findings we support, here we focus on  $Y\pi$  and the comparison between the two mechanisms.

For most of the results we have selected a light,  $^{16}\text{O}$ , and a medium size,  $^{40}\text{Ar}$ , nucleus, both present in modern neutrino detectors. Furthermore, we also discuss how the cross section depends on the mass number. All results presented here are obtained for muonic antineutrinos.

#### A. Integrated cross sections

Integrated cross sections on  $^{16}\text{O}$  and  $^{40}\text{Ar}$  as a function of  $E_{\bar{\nu}}$  are shown in Fig. 1 for  $\Lambda$  and  $\Sigma^{+,-,0}$  in the final state. Results without and with FSI are displayed. We observe the clear dominance of  $\Lambda$  production. This channel has a substantially larger cross section than the other ones taken together. This is partly due to FSI which favors  $\Sigma \rightarrow \Lambda$  transitions. Thus, we can see that  $\Lambda$

production is slightly enhanced by FSI<sup>4</sup> whereas  $\Sigma^-$  and  $\Sigma^0$  production are diminished. The case of  $\Sigma^+$  is especial because there is no direct QE production. Therefore, for  $E_{\bar{\nu}} < 1.2$  GeV the cross section comes predominantly from FSI.

For both  $\Lambda$  and  $\Sigma^-$ , QE mechanisms are clearly larger than the  $Y\pi$  ones at the examined range of energies. The situation is different for  $\Sigma^0$ , where the cross sections are already comparable at the upper end. In the  $\Sigma^+$  case,  $\Sigma^+\pi$  primary production becomes gradually dominant for  $E_{\bar{\nu}} > 1.2$  GeV. Moreover, in all channels, the higher threshold implies that the  $Y\pi$  mechanisms start to contribute at higher energies but their contributions grow faster. This is very clearly visible in the  $\Sigma^0$  case. Overall, the inelastic mechanisms studied here provide a substantial part of the hyperon production cross section and neglecting them would lead to a serious underestimation of strangeness production induced by antineutrinos.

We should recall that the present model for the inelastic  $Y\pi$  processes incorporates the decuplet resonance  $\Sigma^*(1385)$ , which provides the biggest contribution to  $\Lambda\pi$  production [41]. However, the model does not include the  $s$ -wave  $\Lambda(1405)$  resonance. The comparisons between the results of Ref. [41] and [42] show that  $\Lambda(1405)$  plays a moderate role in  $\Sigma\pi$  production at low energies [41]. However, the  $\Lambda\pi$  channel is not affected by the  $\Lambda(1405)$  resonance, which only decays to  $\Sigma\pi$  and  $\bar{K}N$ . Furthermore,  $\Lambda(1405)$  mechanisms are dominated by  $s$ -waves and grow rather slowly as a function of the energy. As a consequence, after the inspection of Refs. [41, 42], we conclude that they would only be competitive with the  $\Sigma\pi$  inelastic production mechanisms considered here for the  $\Sigma^{-,0}$  and at energies  $E_{\bar{\nu}} < 1.4$  GeV, where QE production is anyway much larger. Thus, we neglect  $\Lambda(1405)$  excitation, as its net contribution would be small while keeping in mind that it could be relevant for the study of  $\Sigma\pi$  exclusive channels where the pion is detected in coincidence with the hyperon.

In Fig. 2, we compare the integrated cross section for  $\Lambda\pi$  production on symmetric nuclei like  $^{12}\text{C}$ ,  $^{16}\text{O}$  and  $^{40}\text{Ca}$  versus two asymmetric ones,  $^{40}\text{Ar}$  and  $^{56}\text{Fe}$ . To render the comparison clearer, the cross sections are divided by the mass number. We observe that the cross sections per nucleon without FSI are almost indistinguishable among nuclei of the same category (symmetric or asymmetric), but somewhat larger for asymmetric ones. This is because the cross section for  $\Lambda\pi$  production off free neutrons is exactly twice the one off protons, as shown in Fig. 4 of Ref. [41].

When FSI and the  $\Lambda$  potential are taken into account, the cross sections per nucleon get enhanced at upper end of the antineutrino energy range under consideration. This increase, which is also larger for asymmetric

<sup>4</sup> If events with  $\Lambda$  hyperons trapped in the mean field potential were counted, the  $\Lambda$ -production cross section would be increased by about 20% (30%) in  $^{16}\text{O}$  ( $^{40}\text{Ar}$ ).

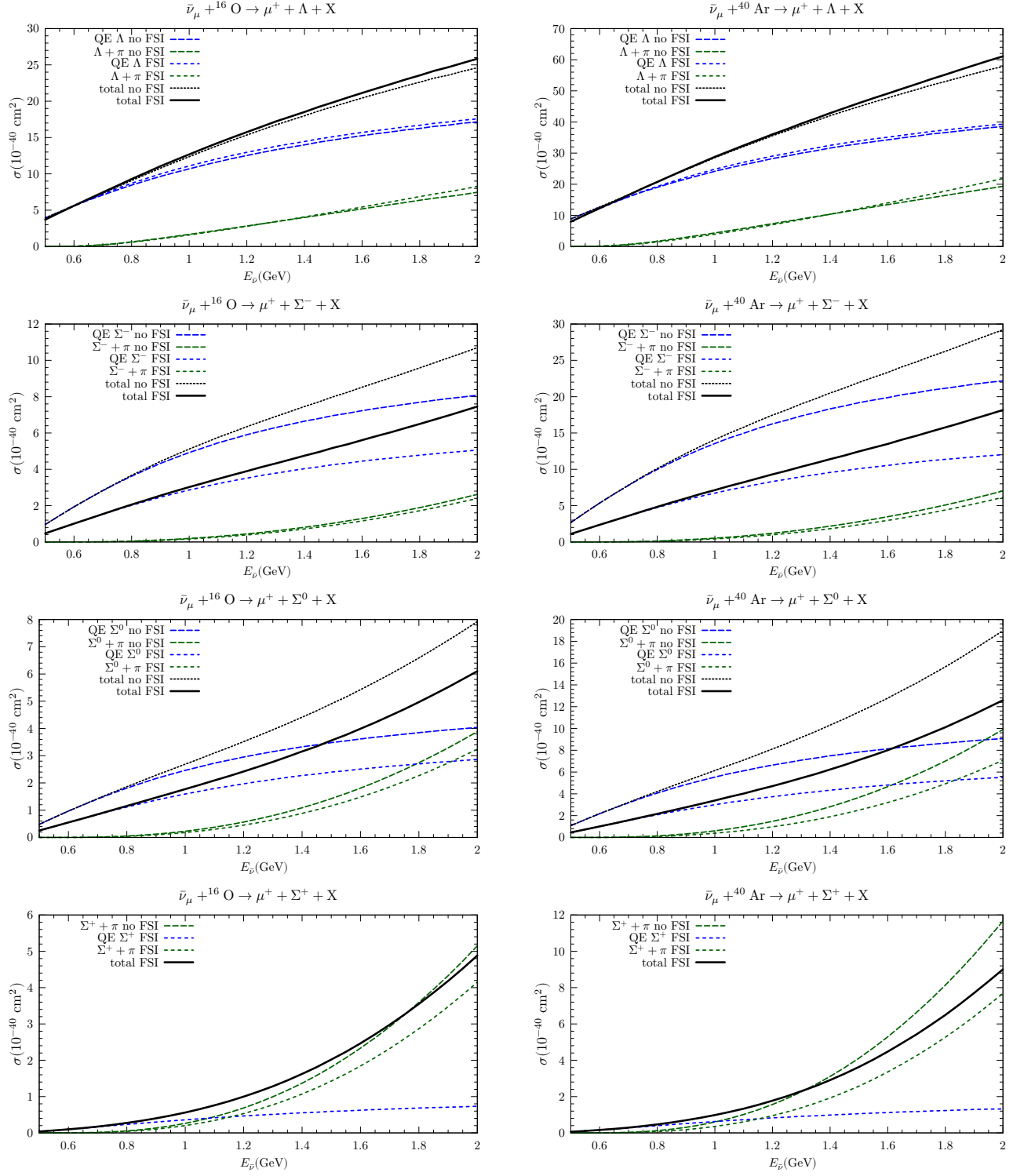


FIG. 1. Integrated cross sections for quasielastic hyperon production, inelastic hyperon-pion production and their sum on  $^{16}\text{O}$  (left) and  $^{40}\text{Ar}$  (right) as a function of the Laboratory  $\bar{\nu}_\mu$  energy. Results with and without hyperon FSI are displayed. Note that  $\Sigma^+$  arise from QE collisions only following FSI.

nuclei is caused by  $\Sigma \rightarrow \Lambda$  conversion. In contrast, a very small reduction can be noticed, particularly for asymmetric nuclei, which can be attributed to the presence of the

attractive potential, on which some of the slow  $\Lambda$  get trapped. It is worth noticing that the scaling with the number of nucleons is largely preserved in presence of

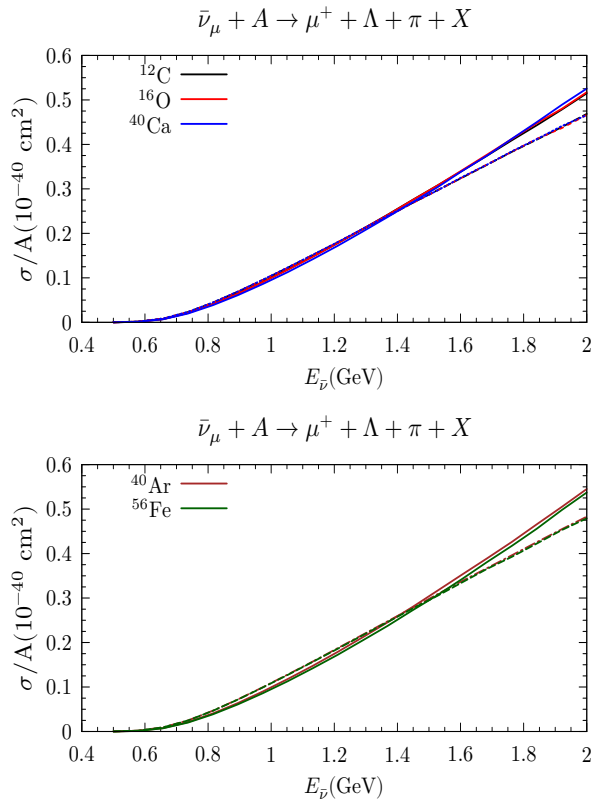


FIG. 2. Integrated cross sections per nucleons for  $\Lambda\pi$  production as a function of the antineutrino energy for a selection of symmetric ( $^{12}\text{C}$ ,  $^{16}\text{O}$  and  $^{40}\text{Ca}$ ) (top panel) and asymmetric nuclei ( $^{40}\text{Ar}$  and  $^{56}\text{Fe}$ ) (bottom panel). Dashed (solid) lines are obtained without (with) FSI.

### FSI.

We have also estimated the fraction of absorbed pions in the way explained at the end of the previous section. As expected, it grows with the nuclear mass number once pions have to travel longer in heavier nuclei, which increases the absorption probability. On the other hand, this fraction decreases with the incident antineutrino energy: the absorption probability increases for slower (in average) pions. More quantitatively, 55-70% of the produced pions are absorbed at  $E_{\bar{\nu}} = 1$  GeV and 30-50% at 2 GeV for the targets considered in this study ( $^{12}\text{C}$ ,  $^{16}\text{O}$ ,  $^{40}\text{Ca}$ ,  $^{40}\text{Ar}$  and  $^{56}\text{Fe}$ ).

### B. Hyperons energy distributions

In Fig. 3, we show hyperon kinetic energy distributions for  $^{16}\text{O}$  at  $E_{\bar{\nu}} = 1, 2$  GeV. The incoming antineutrino energy of 1 GeV and target have been chosen to facilitate the comparison of our results with previous studies of QE hyperon production [35, 48]. The higher energy, 2 GeV, examines a kinematic region where  $Y\pi$  mechanisms are more relevant. The shaded bands in Fig. 3 correspond to hyperon kinetic energies  $T_Y \leq 50$  MeV. As previously

discussed, for hyperon low energies the semiclassical approximation adopted for FSI is questionable. Even if less accurate, we show results in this low energy region as they reflect the amount of produced hyperons and the impact of the  $\Lambda$  potential and FSI.

For the QE mechanism, in the absence of the  $\Lambda$  potential, we have checked that our results are fully consistent with those of Ref. [48]<sup>5</sup>. As it was also seen in Fig. 1, at 1 GeV QE contributions are much larger than  $Y\pi$  production except for the  $\Sigma^+$  channel, where primary QE production is absent. In this case, for hyperon kinetic energies just above 100 MeV, inelastic mechanisms compete with QE  $\Sigma^+$  production. In the other three channels changes caused by the  $Y\pi$  mechanisms are minor.

At 2 GeV the relative importance of the  $Y\pi$  mechanisms is larger. They become dominant for  $\Sigma^+$  production except at low  $T_Y$ . Even for the  $\Sigma^0$  they are the main contribution above 300 MeV.

This figure clearly illustrates the consequences of FSI. Not only many of the hyperons mutate into another species. There is also a clear shape distortion caused by a significant event displacement towards low kinetic energies because in each interaction hyperons transfer a fraction of their energy to the scattered nucleon. In fact, the energy distributions in presence of FSI are peaked at low energies. This feature is most important for  $\Sigma^+$ , a large fraction of which are emitted after FSI. In the case of  $\Lambda$  production, the impact of the potential is significant at low energies, where it leads to changes in the energy spectra. After FSI, many  $\Lambda$  hyperons have kinetic energies smaller than the absolute value of the local mean field potential and therefore, as explained in Sec. II E, are not counted as asymptotic states. We do not dwell on the details of the shape of  $\Lambda$  kinetic energy distributions at  $T_\Lambda \leq 50$  MeV, also obtained in Ref. [47], because, as explained, the semiclassical treatment is not realistic at these energies.

### C. Angular distributions

We have examined angular distributions for the relative angle between final hyperon and lepton momenta,  $\theta_{Yl}$ .<sup>6</sup> We have found that  $d\sigma/d\cos\theta_{Yl}$  is particularly sensitive to the production mechanisms, showing a different behavior for QE and  $Y\pi$  processes. This distinctive feature could help to disentangle them using data and study their relative importance.

Some illustrative results are presented in Fig. 4. For all channels, the  $Y\pi$  contributions are forward peaked and display a monotonous growth as a function of  $\cos\theta_{Yl}$ . On the other hand, for QE processes there is a bump around

<sup>5</sup> There are some discrepancies with the FSI curves of Ref. [35] because of a wrong implementation of the Pauli blocking which led to an underestimation of FSI effects in that study.

<sup>6</sup> Pions are treated inclusively: they might be emitted or absorbed.

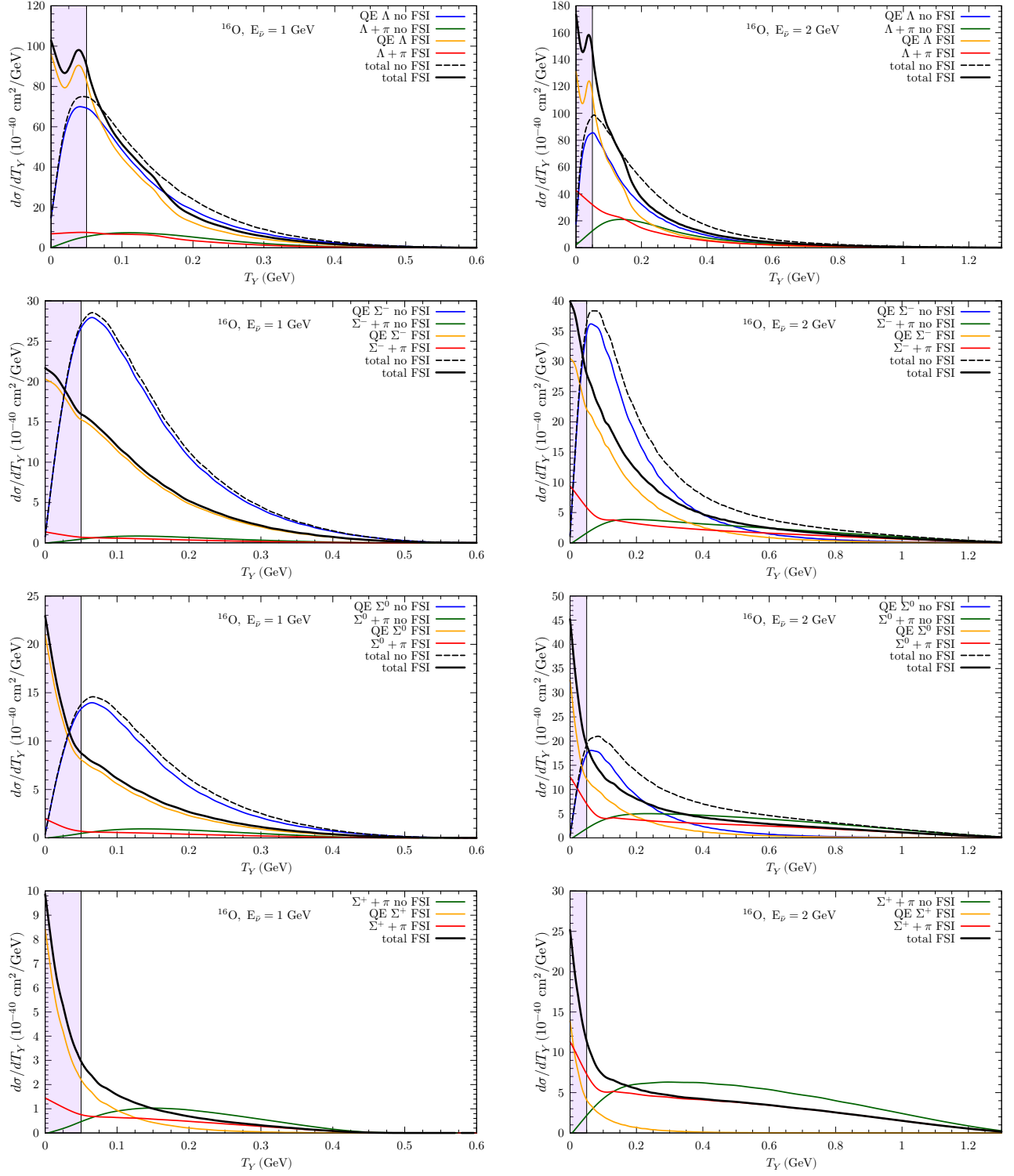


FIG. 3. Hyperon kinetic energy distributions for quasielastic hyperon production, inelastic hyperon-pion production and their sum, computed for  $\bar{\nu}_\mu + {}^{16}\text{O} \rightarrow \mu^+ + Y + X$ , with and without FSI, at fixed antineutrino energies of  $E_{\bar{\nu}} = 1$  GeV (left panels) and  $E_{\bar{\nu}} = 2$  GeV (right panels). The shaded areas correspond to  $T_Y \leq 50$  MeV.

$\cos\theta_{Yl} \approx 0.4$ , which is also present in the total cross section. This peak, mostly driven by phase space, exists for QE processes on single nucleons. It is also present

when vector and axial parts of the hadronic current are separately considered. The peak position hardly changes with the neutrino energy and is largely unaffected by FSI.



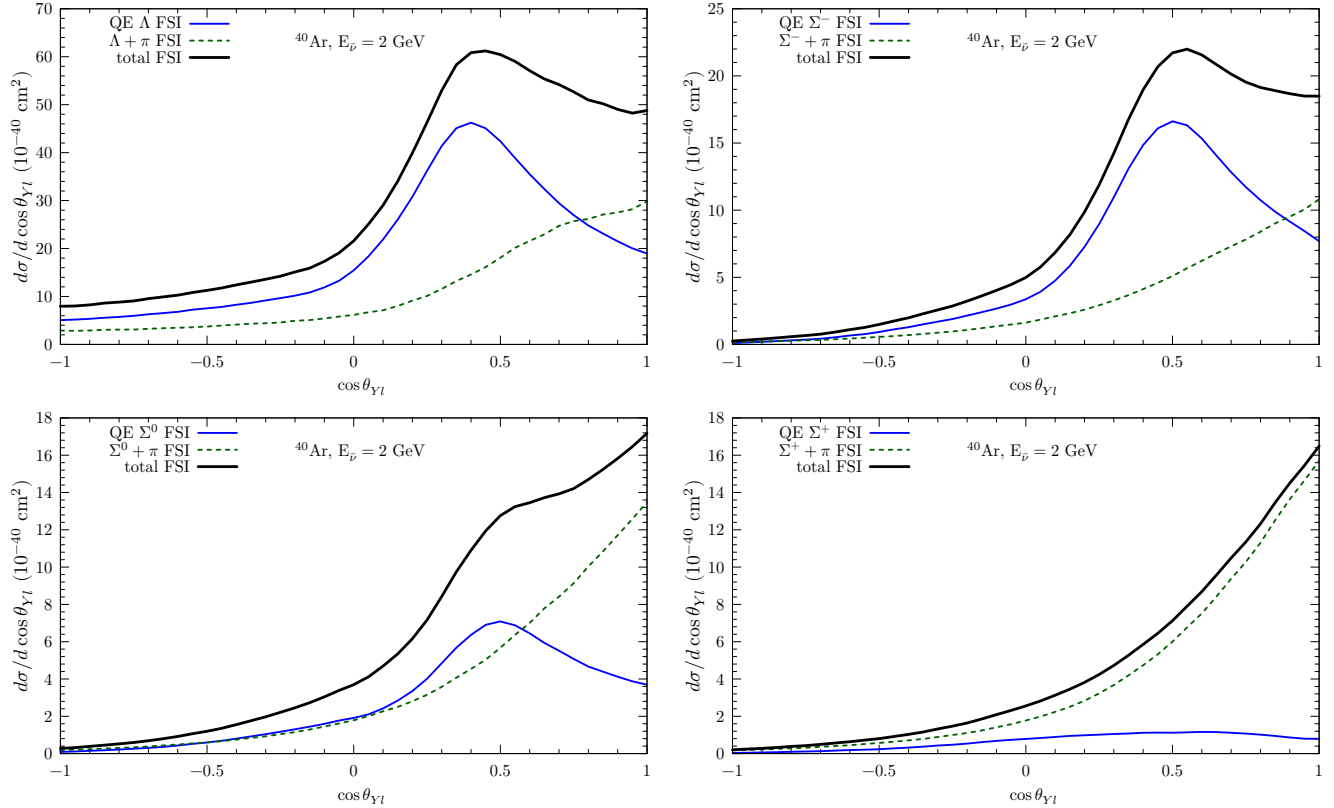


FIG. 4. Angular distributions for the cosine of the angle between hyperon and muon in  $\bar{\nu}_\mu + {}^{40}\text{Ar} \rightarrow \mu^+ + Y + X$ . Solid blue lines correspond to QE reactions, dashed lines to  $Y\pi$  production, and solid black ones to their sum. All the curves include FSI and the  $\Lambda$  nuclear potential.

The presence of such a structure for the QE mechanism and its properties are in line with the findings of Ref. [47] as can be seen in Figs. 23 and 24 of that reference. As shown in Fig. 4 up to  $E_{\bar{\nu}} = 2$  GeV the peak remains visible in the sum of QE and  $Y\pi$  for all hyperons except for  $\Sigma^+$  because the QE contribution is too small.

#### D. Comparison with the MicroBooNE measurement

As discussed in the Introduction, the experimental information for weak hyperon production is very scarce but a new scenario awaits with SBND at FNAL, which is expected to accumulate 8000  $\Lambda$  and 4500  $\Sigma^+$  in only three years of operation [33, 34]<sup>7</sup>.

In the mean time, MicroBooNE has reported five  $\Lambda$  events over the background from the exposure of its liquid argon time projection chamber to the off-axis NUMI beam [32], and a fourfold increase with already collected

data is expected [32]. Driven by these prospects we have studied  $\Lambda$  production on argon in the conditions of the MicroBooNE measurement. Clearly, the statistics is still too low to discriminate between models or to attempt the extraction of transition form factors or other parameters of the theory but the available data already provide useful information.

In Fig. 5 (left), we plot the differential cross section for  $\Lambda$  production as a function of the hyperon kinetic energy averaged over the flux used by MicroBooNE in their simulations. Its shape is available from the Supplemental Material of Ref. [32]. With respect to the distribution without FSI, a clear enhancement at low kinetic energies is apparent which reveals a strong  $\Sigma \rightarrow \Lambda$  conversion. The QE contribution is predominant while the  $Y\pi$  one brings only a minor increase. According to our estimates based on Eq. 15, half of the primarily produced pions will be absorbed and the rest are part of the final hadronic system  $X$  without strange particles. However, the MicroBooNE measurement has phase space restrictions dictated by the detection thresholds of the  $\Lambda \rightarrow p\pi^-$  decay products used to identify the hyperon. To correct for this we multiply our prediction by the fraction of  $\Lambda$  decays with  $p$  and  $\pi^-$  above detection threshold. This quantity as a function of the hyperon momentum is readily provided by MicroBooNE in the Supplemental Material

<sup>7</sup> This estimate was obtained by the SBND collaboration using the GENIE event generator [60] for a  $6.6 \times 10^{20}$  protons on target exposure.

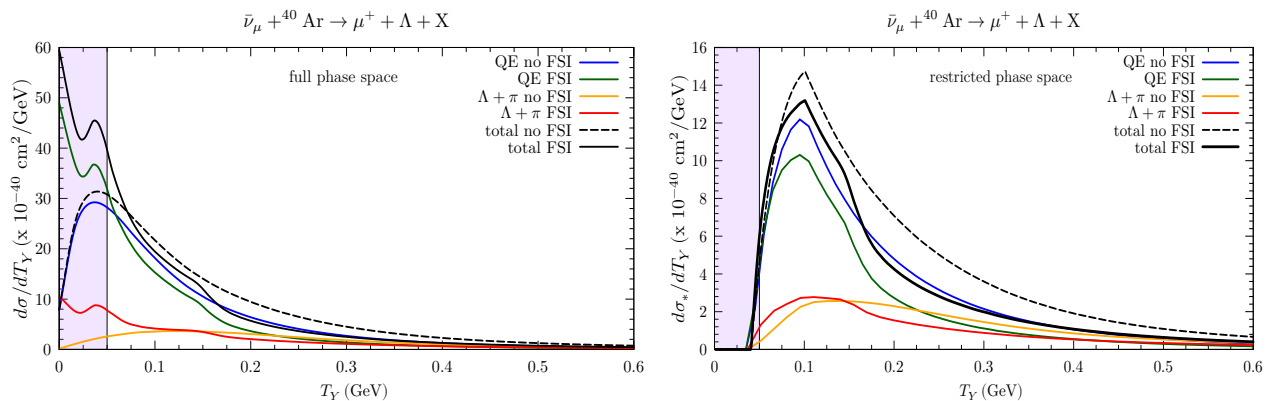


FIG. 5.  $\Lambda$  kinetic energy spectra averaged over the NUMI flux at MicroBooNE without (left) and with (right) experimental phase space restrictions [32]. Contributions from QE and  $Y\pi$  mechanisms and their sum, with and without FSI, are shown.

of Ref. [32]. The result is displayed in the right panel of Fig. 5. One immediately notices that the detector is blind to  $\Lambda$  with  $T_\Lambda < 40$  MeV, accounting for a large fraction of the cross section. The opportunity to understand better FSI and test models in this challenging region is unfortunately missed. Interestingly, this physics will be enabled in large-volume pressurized argon time projection chambers such as the one under development by DUNE [61, 62], where reconstruction thresholds in the few-MeV range are anticipated for hadrons.

On the other hand, in the restricted phase space, the relative importance of the  $Y\pi$  mechanism as a source of pions is considerably enhanced. In fact, as can be seen in Table I, the  $Y\pi$  contribution accounts to one third of the total flux-averaged cross section in the restricted phase space,  $\sigma_*$ . The value of  $\sigma_*$  we obtain, including both

	$\sigma_* (\times 10^{-40} \text{ cm}^2/\text{Ar})$
MicroBooNE	$2.0^{+2.1}_{-1.6}$
QE + $Y\pi$ , full model	2.13
QE	1.44
$Y\pi$	0.69

TABLE I. Flux-averaged cross section for  $\Lambda$  production on argon in the restricted phase space,  $\sigma_*$  defined in Ref. [32]. The experimental value measured by MicroBooNE is compared to our result, for which the QE and  $Y\pi$  contributions are separately given.

QE and  $Y\pi$  contributions, agrees with the MicroBooNE experimental result, whose discriminating power is still limited by the low statistics. According to Ref. [32], the measured  $\sigma_*$  value is also consistent with the predictions from the GENIE [60] and NuWro [47] event generators. It should be however remarked that neither of these two event generators includes  $Y\pi$  channels<sup>8</sup>. Our findings

imply that the  $\Lambda\pi$  contribution, which is dominated by  $\Sigma^*(1385)$  excitation, is a very important ingredient for the analysis and interpretation of the experimental results awaited at MicroBooNE and SBND.

#### IV. SUMMARY AND CONCLUSIONS

We have studied hyperon production on nuclei induced by antineutrinos, in the energy region where associated strangeness production ( $\Delta S = 0$ ) and secondary hyperon production induced by  $\bar{K}$  are still negligible.

These reactions proceed mostly via quasielastic scattering in which the emission of a charged lepton and a hyperon is induced by antineutrino-nucleon interactions. These mechanisms have been earlier studied, exploring their sensitivity to the nucleon-to-hyperon transition form factors, SU(3) symmetry breaking or the existence of second class currents.

In this work, we have also investigated an additional type of processes which contributes to the inclusive hyperon production cross section. Namely, the case in which a pion is emitted together with a  $\Sigma$  or  $\Lambda$ . The extra pion mass implies a higher threshold than in the QE mechanisms but, nevertheless, these  $Y\pi$  processes start to be relevant at much lower energies than  $YK$  production and their cross sections grow faster with the antineutrino energy than the QE ones. Moreover, the  $\Sigma^*(1385)$ , which decays strongly into  $\Lambda\pi$  and  $\Sigma\pi$ , is located close to threshold.

Nuclear effects have been taken into account using the impulse approximation and a local Fermi gas description of the initial state. An attractive nuclear mean field potential for  $\Lambda$  hyperons has also been incorporated. The final state interaction between the produced hyperon and the nucleon spectators has been accounted for with a Monte Carlo intranuclear cascade. As a consequence of hyperon FSI, there is an enhancement in  $\Lambda$  production caused by  $\Sigma \rightarrow \Lambda$  conversion. In addition, primary produced hyperons lose energy when they collide with nucle-

<sup>8</sup> In addition, GENIE does not take FSI into account.

ons and, thus, energy distributions are strongly shifted towards low energies. Instead, lepton-hyperon angular distributions are only slightly softened by FSI.

We find that  $Y\pi$  channels are relevant for the description of the hyperon production off nuclei. Indeed, they provide the main contribution to  $\Sigma^+$  production and generate a sizable fraction of the total cross section in other channels. Their relative importance increases with energy. Failure to account for these mechanisms would introduce biases in the experimental analysis and interpretation of experimental results. This will be the case, for example, in attempts to constrain nucleon-to-hyperon transition form factors or extract information about hyperon potentials using neutrino scattering.  $Y\pi$  events could be discriminated by detecting the emitted pions but this will not be possible for a large fraction of these events because of pion intranuclear absorption and detection thresholds. In this context we have obtained that distributions over the lepton-hyperon relative angles are useful observables for distinguishing between QE and  $Y\pi$  processes. In any respect, adequate consideration of inelastic  $Y\pi$  production in the event generators used by experiments, such as GENIE or NuWro, would be required.

Finally, we have studied  $\Lambda$  production on argon in the conditions of the recent MicroBooNE measurement. This implies folding with the antineutrino flux and imposing the proper acceptance cuts. The relative high detection threshold and small acceptance for low energy  $\Lambda$  strongly reduces the fraction of events that can be identified, and increases the relative importance of inelastic  $Y\pi$  with respect to QE ones. In our result for the phase space restricted flux averaged cross section, which is consistent with the low-statistics experimental value, the  $\Lambda\pi$  mech-

anism accounts for one third of the total.

More data on hyperon production from MicroBooNE and SBND are eagerly awaited to learn more about this rare but interesting process.

## V. ACKNOWLEDGEMENTS

The authors acknowledge the use of resources from the scientific computing cloud PROTEUS of the Instituto Interuniversitario Carlos I de Física Teórica y Computacional of the University of Granada to perform some of the numerical calculations required in this study. They also thank J. Nowak and C. Thorpe for very useful communications regarding hyperon production measurements at MicroBooNE, and D. González-Díaz for valuable insight about argon time projection chambers. The authors are also grateful to Prof. J. T. Sobczyk for other useful information.

This work has been partially supported by the Spanish Ministry of Science under grants PID2020-114767GB-I00 and PID2020-112777GB-I00, funded by MCIN/AEI/10.13039/501100011033. It has also been funded by FEDER/Junta de Andalucía-Consejería de Transformación Económica, Industria, Conocimiento y Universidades/A-FQM-390-UGR20, by the Junta de Andalucía (grant No. FQM-225) and by Generalitat Valenciana under contract PROMETEO/2020/023 and the “Planes Complementarios de I+D+i” program (grant ASFAE/2022/022) by MCIN with funding from the European Union NextGenerationEU and Generalitat Valenciana. M.B.G. also acknowledges support from Spanish Ministry of Science under grant PRE2018-083794 funded by MCIN/AEI/10.13039/501100011033 and by “ESF Investing in your future”.

- 
- [1] N. Cabibbo, Unitary Symmetry and Leptonic Decays, *Phys. Rev. Lett.* **10**, 531 (1963).
  - [2] R. L. Workman *et al.* (Particle Data Group), Review of Particle Physics, *PTEP* **2022**, 083C01 (2022).
  - [3] N. Cabibbo and F. Chilton, Hyperon Production by Neutrinos in an  $SU_3$  Model, *Phys. Rev.* **137**, B1628 (1965).
  - [4] C. H. Llewellyn Smith, Neutrino Reactions at Accelerator Energies, *Phys. Rept.* **3**, 261 (1972).
  - [5] N. Cabibbo, E. C. Swallow, and R. Winston, Semileptonic hyperon decays, *Ann. Rev. Nucl. Part. Sci.* **53**, 39 (2003), [arXiv:hep-ph/0307298](#).
  - [6] P. E. Shanahan, A. N. Cooke, R. Horsley, Y. Nakamura, P. E. L. Rakow, G. Schierholz, A. W. Thomas, R. D. Young, and J. M. Zanotti,  $SU(3)$  breaking in hyperon transition vector form factors, *Phys. Rev. D* **92**, 074029 (2015), [arXiv:1508.06923 \[nucl-th\]](#).
  - [7] S. Sasaki, Hyperon vector form factor from 2+1 flavor lattice QCD, *Phys. Rev. D* **86**, 114502 (2012), [arXiv:1209.6115 \[hep-lat\]](#).
  - [8] S. Sasaki, Continuum limit of hyperon vector coupling  $f_1(0)$  from 2+1 flavor domain wall QCD, *Phys. Rev. D* **96**, 074509 (2017), [arXiv:1708.04008 \[hep-lat\]](#).
  - [9] S.-L. Zhu, S. Puglia, and M. J. Ramsey-Musolf, Recoil order chiral corrections to baryon octet axial currents, *Phys. Rev. D* **63**, 034002 (2001), [arXiv:hep-ph/0009159](#).
  - [10] A. Lacour, B. Kubis, and U.-G. Meissner, Hyperon decay form-factors in chiral perturbation theory, *JHEP* **10**, 083, [arXiv:0708.3957 \[hep-ph\]](#).
  - [11] T. Ledwig, J. Martin Camalich, L. S. Geng, and M. J. Vicente Vacas, Octet-baryon axial-vector charges and  $SU(3)$ -breaking effects in the semileptonic hyperon decays, *Phys. Rev. D* **90**, 054502 (2014), [arXiv:1405.5456 \[hep-ph\]](#).
  - [12] U. Sauerwein, M. F. M. Lutz, and R. G. E. Timmermans, Axial-vector form factors of the baryon octet and chiral symmetry, *Phys. Rev. D* **105**, 054005 (2022), [arXiv:2105.06755 \[hep-ph\]](#).
  - [13] R. Flores-Mendieta, E. E. Jenkins, and A. V. Manohar,  $SU(3)$  symmetry breaking in hyperon semileptonic decays, *Phys. Rev. D* **58**, 094028 (1998), [arXiv:hep-ph/9805416](#).
  - [14] A. J. Buchmann and R. F. Lebed, Baryon charge radii

- and quadrupole moments in the  $1/N(c)$  expansion: The three flavor case, *Phys. Rev. D* **67**, 016002 (2003), [arXiv:hep-ph/0207358](#).
- [15] A. Calle Cordon and J. L. Goity, Baryon Masses and Axial Couplings in the Combined  $1/N_c$  and Chiral Expansions, *Phys. Rev. D* **87**, 016019 (2013), [arXiv:1210.2364 \[nucl-th\]](#).
- [16] F. Schlumpf, Beta decay of hyperons in a relativistic quark model, *Phys. Rev. D* **51**, 2262 (1995), [arXiv:hep-ph/9409272](#).
- [17] G. Ramalho and K. Tsushima, Axial form factors of the octet baryons in a covariant quark model, *Phys. Rev. D* **94**, 014001 (2016), [arXiv:1512.01167 \[hep-ph\]](#).
- [18] G.-S. Yang and H.-C. Kim, Hyperon Semileptonic decay constants with flavor SU(3) symmetry breaking, *Phys. Rev. C* **92**, 035206 (2015), [arXiv:1504.04453 \[hep-ph\]](#).
- [19] X. Y. Liu, A. Limphirat, K. Xu, Z. Zhao, K. Khosonthongkee, and Y. Yan, Axial transition form factors of octet baryons in the perturbative chiral quark model, *Phys. Rev. D* **107**, 074006 (2023), [arXiv:2209.00808 \[hep-ph\]](#).
- [20] T. Eichten *et al.*, Observation of 'Elastic' Hyperon Production by Anti-neutrinos, *Phys. Lett. B* **40**, 593 (1972).
- [21] O. Erriquez *et al.*, Strange Particle Production by anti-neutrinos, *Phys. Lett. B* **70**, 383 (1977).
- [22] O. Erriquez *et al.*, Production of Strange Particles in anti-neutrino Interactions at the CERN PS, *Nucl. Phys. B* **140**, 123 (1978).
- [23] S. J. Barish *et al.*, Strange-Particle Production in Neutrino Interactions, *Phys. Rev. Lett.* **33**, 1446 (1974).
- [24] G. Fanourakis, L. K. Resvanis, G. Grammatikakis, P. Tsilimigras, A. Vayaki, U. Camerini, W. F. Fry, R. J. Loveless, J. H. Mapp, and D. D. Reeder, Study of Low-energy Anti-neutrino Interactions on Protons, *Phys. Rev. D* **21**, 562 (1980).
- [25] N. J. Baker, P. L. Connolly, S. A. Kahn, H. G. Kirk, M. J. Murtagh, R. B. Palmer, N. P. Samios, and M. Tanaka, Strange Particle Production from Neutrino Interactions in the BNL 7-Ft Bubble Chamber, *Phys. Rev. D* **24**, 2779 (1981).
- [26] V. V. Ammosov *et al.*, Neutral Strange Particle Exclusive Production in Charged Current High-energy Anti-neutrino Interactions, *Z. Phys. C* **36**, 377 (1987).
- [27] D. Son *et al.*, Quasielastic Charmed Baryon Production and Exclusive Strange Particle Production by High-energy Neutrinos, *Phys. Rev. D* **28**, 2129 (1983).
- [28] J. Brunner *et al.* (SKAT), Quasielastic Nucleon and Hyperon Production by Neutrinos and Anti-neutrinos With Energies Below 30-GeV, *Z. Phys. C* **45**, 551 (1990).
- [29] J. A. Formaggio and G. P. Zeller, From eV to EeV: Neutrino Cross Sections Across Energy Scales, *Rev. Mod. Phys.* **84**, 1307 (2012), [arXiv:1305.7513 \[hep-ex\]](#).
- [30] P. Astier *et al.* (NOMAD), Measurement of the Lambda polarization in  $\nu/\mu$  charged current interactions in the NOMAD experiment, *Nucl. Phys. B* **588**, 3 (2000).
- [31] D. Naumov *et al.* (NOMAD), A Study of strange particles produced in neutrino neutral current interactions in the NOMAD experiment, *Nucl. Phys. B* **700**, 51 (2004), [arXiv:hep-ex/0409037](#).
- [32] P. Abratenko *et al.* (MicroBooNE), First measurement of quasi-elastic  $\Lambda$  baryon production in muon anti-neutrino interactions in the MicroBooNE detector, (2022), [arXiv:2212.07888 \[hep-ex\]](#).
- [33] D. Brailsford (SBND), Physics Program of the Short-Baseline Near Detector, *J. Phys. Conf. Ser.* **888**, 012186 (2017).
- [34] P. A. Machado, O. Palamara, and D. W. Schmitz, The Short-Baseline Neutrino Program at Fermilab, *Ann. Rev. Nucl. Part. Sci.* **69**, 363 (2019), [arXiv:1903.04608 \[hep-ex\]](#).
- [35] S. K. Singh and M. J. Vicente Vacas, Weak quasi-elastic production of hyperons, *Phys. Rev. D* **74**, 053009 (2006).
- [36] M. Rafi Alam, S. Chauhan, M. Sajjad Athar, and S. K. Singh,  $\bar{\nu}_l$  induced pion production from nuclei at  $\sim 1$  GeV, *Phys. Rev. D* **88**, 077301 (2013), [arXiv:1310.7704 \[nucl-th\]](#).
- [37] A. Fatima, M. S. Athar, and S. K. Singh,  $\bar{\nu}_\mu$  induced quasielastic production of hyperons leading to pions, *Eur. Phys. J. ST* **230**, 4391 (2021), [arXiv:2106.14590 \[hep-ph\]](#).
- [38] S. L. Mintz and L.-L. Wen, The weak production of Lambda particles in antineutrino-proton scattering and the contributions of the form factors, *Nucl. Phys. A* **766**, 219 (2006).
- [39] K. S. Kuzmin and V. A. Naumov, Axial mass in reactions of quasielastic antineutrino-nucleon scattering with strange hyperon production, *Phys. Atom. Nucl.* **72**, 1501 (2009).
- [40] H. K. Dewan, Strange Particle Production in Neutrino Scattering, *Phys. Rev. D* **24**, 2369 (1981).
- [41] M. Benitez Galan, M. R. Alam, and I. Ruiz Simo, Cabibbo suppressed single pion production off the nucleon induced by antineutrinos, *Phys. Rev. D* **104**, 073005 (2021), [arXiv:2108.06393 \[hep-ph\]](#).
- [42] X.-L. Ren, E. Oset, L. Alvarez-Ruso, and M. J. Vicente Vacas, Antineutrino induced  $\Lambda(1405)$  production off the proton, *Phys. Rev. C* **91**, 045201 (2015), [arXiv:1501.04073 \[hep-ph\]](#).
- [43] M. R. Alam, I. R. Simo, M. S. Athar, and M. J. Vicente Vacas,  $\bar{\nu}$  induced  $\bar{K}$  production off the nucleon, *Phys. Rev. D* **85**, 013014 (2012), [arXiv:1111.0863 \[hep-ph\]](#).
- [44] R. E. Shrock, Associated Production by Weak Charged and Neutral Currents, *Phys. Rev. D* **12**, 2049 (1975).
- [45] G. B. Adera, B. I. S. Van Der Ventel, D. D. van Niekerk, and T. Mart, Strange-particle production via the weak interaction, *Phys. Rev. C* **82**, 025501 (2010), [arXiv:1112.5748 \[nucl-th\]](#).
- [46] S. X. Nakamura, H. Kamano, and T. Sato, Dynamical coupled-channels model for neutrino-induced meson productions in resonance region, *Phys. Rev. D* **92**, 074024 (2015), [arXiv:1506.03403 \[hep-ph\]](#).
- [47] C. Thorpe, J. Nowak, K. Niewczas, J. T. Sobczyk, and C. Juszczak, Second class currents, axial mass, and nuclear effects in hyperon production, *Phys. Rev. C* **104**, 035502 (2021), [arXiv:2010.12361 \[hep-ph\]](#).
- [48] J. E. Sobczyk, N. Rocco, A. Lovato, and J. Nieves, Weak Production of Strange and Charmed Ground-State Baryons in Nuclei, *Phys. Rev. C* **99**, 065503 (2019), [arXiv:1901.10192 \[nucl-th\]](#).
- [49] O. Lalakulich, K. Gallmeister, and U. Mosel, Neutrino- and antineutrino-induced reactions with nuclei between 1 and 50 GeV, *Phys. Rev. C* **86**, 014607 (2012), [arXiv:1205.1061 \[nucl-th\]](#).
- [50] H. De Vries, C. W. De Jager, and C. De Vries, Nuclear charge and magnetization density distribution parameters from elastic electron scattering, *Atom. Data Nucl. Data Tabl.* **36**, 495 (1987).
- [51] I. Vidana, A. Polls, A. Ramos, and M. Hjorth-Jensen,

- Hyperon properties in finite nuclei using realistic  $Y N$  interactions, *Nucl. Phys. A* **644**, 201 (1998), [arXiv:nucl-th/9805032](#).
- [52] J. L. Rodríguez-Sánchez, J. C. David, J. Hirtz, J. Cugnon, and S. Leray, Constraining the  $\Lambda$ -nucleus potential within the Liège intranuclear cascade model, *Phys. Rev. C* **98**, 021602 (2018).
  - [53] J. Hirtz, J. C. David, A. Boudard, J. Cugnon, S. Leray, I. Leya, J. L. Rodríguez-Sánchez, and G. Schnabel, Strangeness production in the new version of the Liège intranuclear cascade model, *Phys. Rev. C* **101**, 014608 (2020), [arXiv:1909.02246 \[nucl-th\]](#).
  - [54] T. Harada and Y. Hirabayashi, Production spectra with a  $\Sigma^-$  hyperon in  $(\pi^-, K^+)$  reactions on light to heavy nuclei, *Phys. Rev. C* **107**, 054611 (2023).
  - [55] E. Oset and M. J. Vicente-Vacas, Inclusive  $(\pi, 2\pi)$  Reactions in Nuclei, *Nucl. Phys. A* **454**, 637 (1986).
  - [56] S. K. Singh, M. Sajjad Athar, and S. Ahmad, Nuclear effects in neutrino induced coherent pion production at K2K and MiniBooNE, *Phys. Rev. Lett.* **96**, 241801 (2006), [arXiv:nucl-th/0601045](#).
  - [57] X. Zhang and B. D. Serot, Coherent Neutrinoproduction of Photons and Pions in a Chiral Effective Field Theory for Nuclei, *Phys. Rev. C* **86**, 035504 (2012), [arXiv:1208.1553 \[nucl-th\]](#).
  - [58] E. Oset and L. L. Salcedo,  $\Delta$  Selfenergy in Nuclear Matter, *Nucl. Phys. A* **468**, 631 (1987).
  - [59] L. L. Salcedo, E. Oset, M. J. Vicente-Vacas, and C. Garcia-Recio, Computer Simulation of Inclusive Pion Nuclear Reactions, *Nucl. Phys. A* **484**, 557 (1988).
  - [60] C. Andreopoulos *et al.*, The GENIE Neutrino Monte Carlo Generator, *Nucl. Instrum. Meth. A* **614**, 87 (2010), [arXiv:0905.2517 \[hep-ph\]](#).
  - [61] V. Hewes *et al.* (DUNE), Deep Underground Neutrino Experiment (DUNE) Near Detector Conceptual Design Report, *Instruments* **5**, 31 (2021), [arXiv:2103.13910 \[physics.ins-det\]](#).
  - [62] A. Abed Abud *et al.* (DUNE), A Gaseous Argon-Based Near Detector to Enhance the Physics Capabilities of DUNE, (2022), [arXiv:2203.06281 \[hep-ex\]](#).